Modelled light curve variability due to blob injection in RMHD jet simulations

D.M. Kulik, B. van Soelen, I.P. van der Westhuizen

Department of Physics, University of the Free State, Bloemfontein, South Africa

1. Introduction:

Active Galactic Nuclei (AGN) are compact and highly luminous regions at the centre of galaxies. They have been observed to show multi-wavelength variability on time scales of minutes to years. Blob propagation within the relativistic jets of AGN are a possible mechanism for explaining some of the variability. Models describing the formation and subsequent propagation of blobs along the jet column vary from the leptonic blob-in-jet model [1] to compact magnetized blobs produced by red giants that cross the jet close to the central black hole [2].

Previous astrophysical fluid dynamical simulations have been done to model the effects of injecting shocks, perturbations, and blobs into the jet nozzle (e.g. [3]). In this work, by using RMHD simulations, blobs with differing properties were allowed to evolve and their effects on the jet structure and magnetic fields were investigated. A post-processing approximation of the synchrotron emission was applied to calculate the emission and absorption, to investigate how the different blobs will change the emission.

2. Jet and blob simulations & emission modelling:

A 3D jet model was constructed in PLUTO (a computational software for solving astrophysical fluid dynamical problems) [4] consisting of 288 x 768 x 288 grid cells with a resolution of 12 grid cells/jet radius. An under-dense and thermally pressure matched jet model was used. The jet nozzle was generated by a jet-ambient profile using a normalized modified Gumbel distribution [5]. A force-free magnetic field setup was utilized as found in [6] where the poloidal and toroidal components of the magnetic field are given respectively by,

$$B_z = \frac{B_0}{1 + (r/a)^2} \quad (1)$$

$$B_\phi = \frac{(r/a)B_0}{1 + (r/a)^2} \quad (2)$$

where B_0 parametrizes the magnetic field amplitude, r is the distance from the jet centre, and a is the characteristic radius of the jet beam. The environment was set up in Cartesian coordinates and evolved with time using a linear interpolation method, RK2 time stepping, and the HLLD Riemann solver. A list of parameters given in computational units for the jet setup are given in Table 1.

Blobs were formed by altering a single jet parameter (density, velocity, or magnetic field) at the jet nozzle and injected such that the blob evolved in time based on a quasi-spherical radius profile. A list of parameters for the different blob setups are given in Table 2.

A post-processing code similar to [7] was used to find the integrated synchrotron intensity. It was assumed the jet contained an equal number of protons and electrons, and a 10% fraction of the electrons energy density was in a power-law distribution. These assumptions were fixed for each cell within the simulation. The normalization constant was applied from [8], and is given by,

$$K = \left[\frac{U(p-1)}{1 - C_e^{2-p}}\right]^{p-1} \left[\frac{1 - C_e^{1-p}}{N(p-1)}\right]^{p-2} \quad (3)$$

where U is the fractional component of the electron's internal energy density, N is the fractional component of the electron's number density and C_e is the ratio between the maximum and minimum electron energies that follow the single power law distribution. The emission and absorption coefficient approximations were used from [9] and were integrated along the line-of-sight taking into consideration relativistic effects such as Doppler boosting and light-travel time.

The post-processing parameters that were used were: the frequency of the modelled emission (ν = 15x10^9 Hz), the electron index (p = 2.1), the viewing angle of the jet relative to the observer's line-of-sight (θ = 15°), and the ratio between the maximum and minimum energies of the electron's following a single power law distribution (C_e = 10^3).

3. Results:

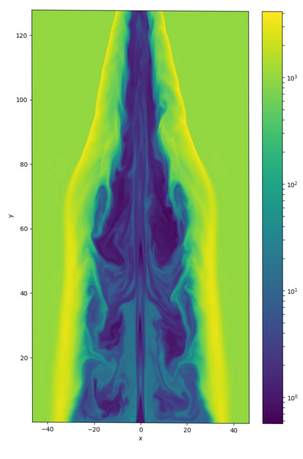

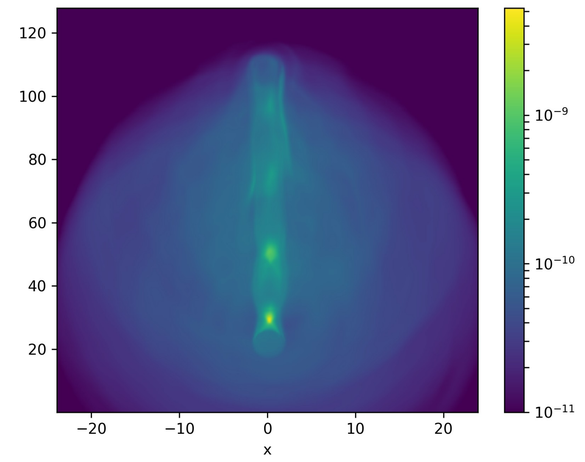

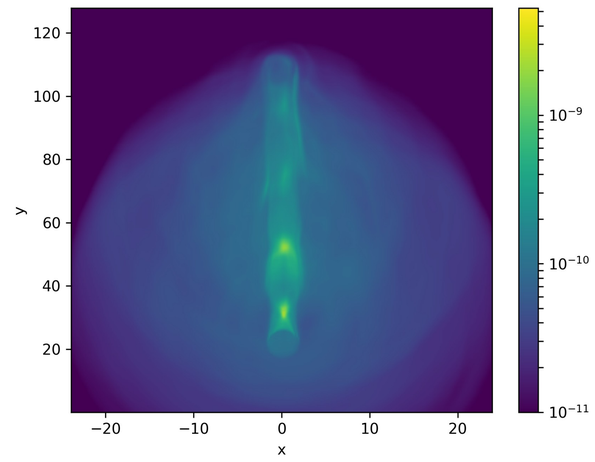

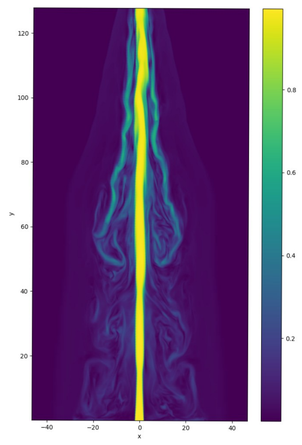

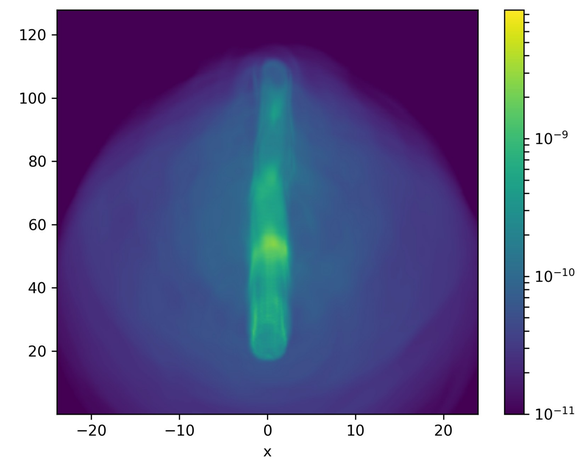

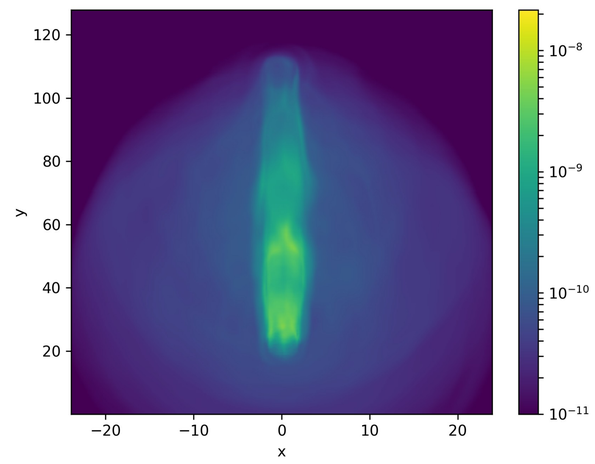

Figure 1: Top: log scaled plot of the density of the jet. Bottom: magnitude of the velocity components of the jet

Figure 2: Integrated intensity plots during different blob injection at 19h with a line-of-sight of 15 degrees from the jet beam being parallel to the viewer. Top left: jet during no blob injection. Top right: velocity blob. Bottom left: density blob. Bottom right: magnetically confined blob. The integrated intensity strength is given in erg cm^{-2} s^{-1} Hz^{-1}

Table 1: Simulation parameters

Parameter	Value
Jet Lorentz factor (Γ_j)	10
Mach number (M)	8
Ambient-Jet density ratio (η)	10^{-3}
Jet density (ρ_j)	1
Magnetic field amplitude (B_0)	0.3
Adiabatic index (γ_{ad})	5/3
Jet, blob, & characteristic radii (r_j, r_b, a)	2, 1, 0.5

Table 2: Blob parameters

Blob type	Value
Density	$10^3\rho_j$
Velocity	$2.5\Gamma_j$
Magnetic	$25B_{0j}$

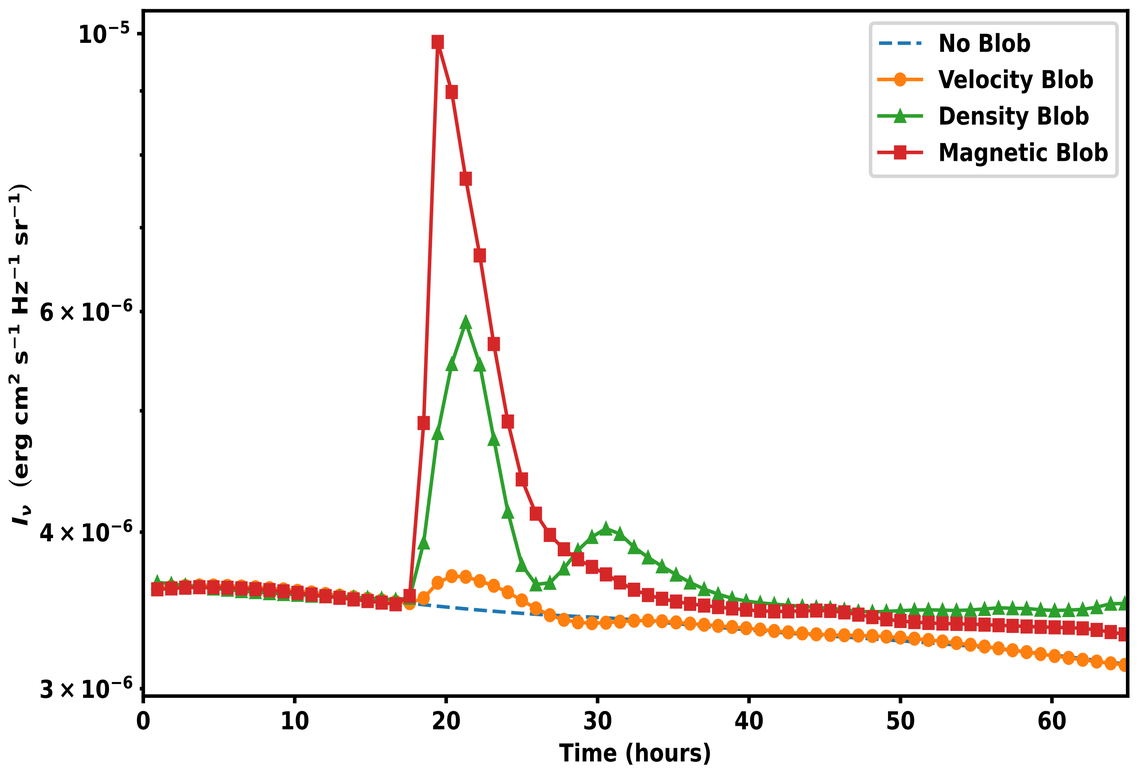

Figure 3: Light curve plot of the integrated intensity over time as different blob types propagated along the jet. This was calculated by summing the specific intensity of all the cells in the simulation domain with respect to time.

4.Discussion and Conclusion:

Each blob type exhibited its own unique light curve showing an increase in the emission from jet quiescence. The velocity blob exhibited the smallest increase. This is due the high Lorentz factor of the blob and the resultant Doppler boosting not being visible from the selected viewing angle. The density blob had the second highest increase. However, it also exhibited a weaker secondary peak which was caused by a strong trailing shock front that persisted behind the density blob, with the shock front propagating outwards into the jet's cocoon region. The strongest peak was generated by the magnetically confined blob and is a result of both a strong toroidal component of the magnetic field along with an additional contribution of the poloidal component of the magnetic field at this viewing angle.

References:

[1] Mücke, A. et al. "BL Lac objects in the synchrotron proton blazar model". Astroparticle Physics 18. (2002): 593-613.
[2] M. V. Barkov, et al. "Rapid TeV variability in blazars as a result of jet-star interaction". The Astrophysical Journal 749. 2(2012): 119.
[3] I. Agudo, et al. "Jet stability and the generation of superluminal and stationary components". The Astrophysical Journal 549. 2(2001): L183–L186.
[4] Mignone et al., "PLUTO: A Numerical Code for Computational Astrophysics", The Astrophysical Journal Supplement Series, Volume 170, Issue 1, pp. 228-242 (2007).
[5] Pratt, J et al., "Extreme-value statistics from Lagrangian convex hull analysis for homogeneous turbulent Boussinesq convection and MHD convection", New Journal of Physics, Volume 19, Issue 6, article id. 065006 (2017).
[6] Y. Mizuno, et al. Three-dimensional relativistic magnetohydrodynamic simulations of current-driven instability. I. INSTABILITY of a static column". The Astrophysical Journal 700. 1(2009): 684–693
[7] I.P. van der Westhuizen et al, "Using synchrotron emission modelling of relativistic hydrodynamic jet simulations to study the FR I/FR II dichotomy of active galactic nuclei radio jets", Monthly Notices of the Royal Astronomical Society,485, no.4 (2019): 4658-4666.
[8] J. L. Gómez, et al. "Parsec-scale synchrotron emission from hydrodynamic relativistic jets in active galactic nuclei". The Astrophysical Journal 449. 1(1995).
[9] G. Ghisellini "Radiative processes in high energy astrophysics". Vol. 873. Springer International Publishing. (2013)

KulikDM@ufs.ac.za | **www.ufs.ac.za** **UFSUV** | **UFSweb** | **UFSweb**

Tenth International Fermi Symposium 2022

9th - 15th October, 2022